Supporting Information

Interfacial Stress Limits PbTe Module Reliability: Porous Fe Foam Mitigates Thermal-Mismatch Stress

Zhoumin Jiang,[a,b] Xiaojian Tan,[*b,c] Zongwei Zhang,[*b] Ailong Yang,[b] Jinqu Feng,[b] Chenhao Han,[b] Lianghan Fan,[b] Jianfeng Cai,[b] Guo-Qiang Liu,[b,c] Jun Jiang[*b,c]

[a.] *School of Material Science and Chemical Engineering, Ningbo University, Ningbo, 315211, China.*

[b.] *Ningbo Institute of Materials Technology and Engineering, Chinese Academy of Sciences, Ningbo, 315201, China*

[c.] *University of Chinese Academy of Sciences, Beijing 100049, China*

Corresponding authors: E-mail: tanxiaojian@nimte.ac.cn; zhangzongwei@nimte.ac.cn; jjun@nimte.ac.cn.

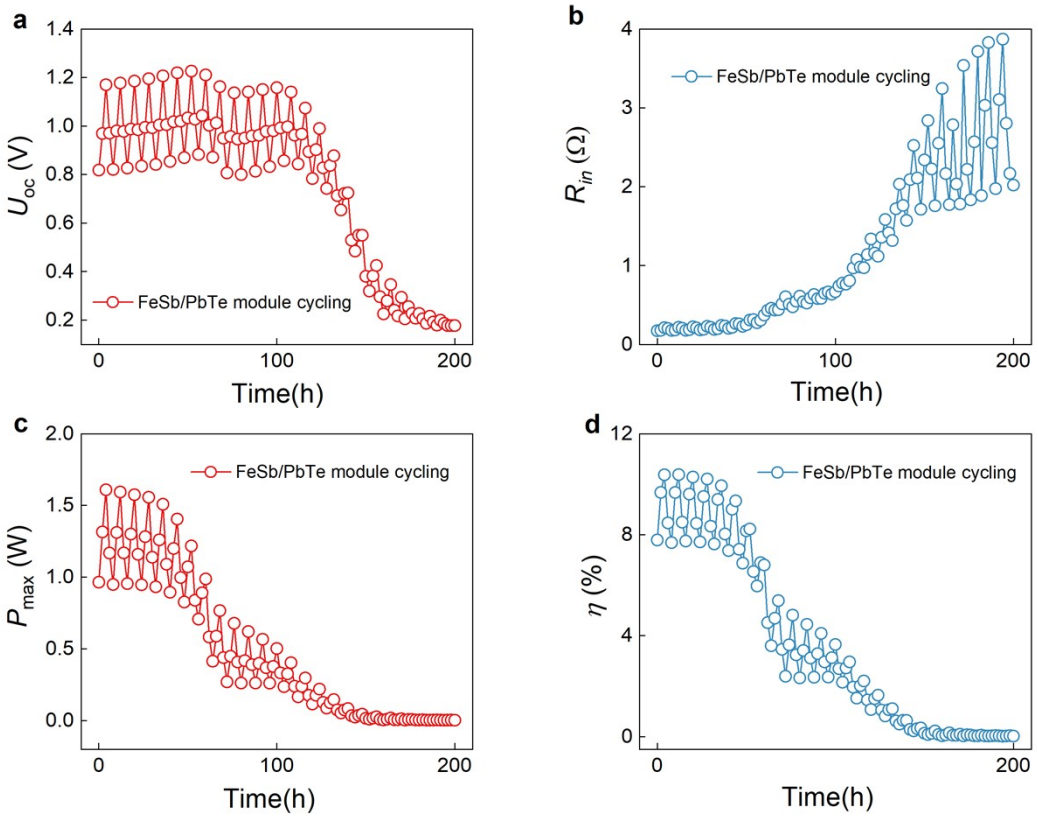

Figure S1. Key parameters of a PbTe-based thermoelectric device featuring an FeSb barrier layer during cyclic thermal stress testing: (a) open-circuit voltage, (b) internal device resistance, (c) maximum output power, and (d) conversion efficiency. The thermal cycling protocol involved varying the hot-side temperature between 643 K and 753 K, with the cold-side temperature maintained at a constant 300 K.

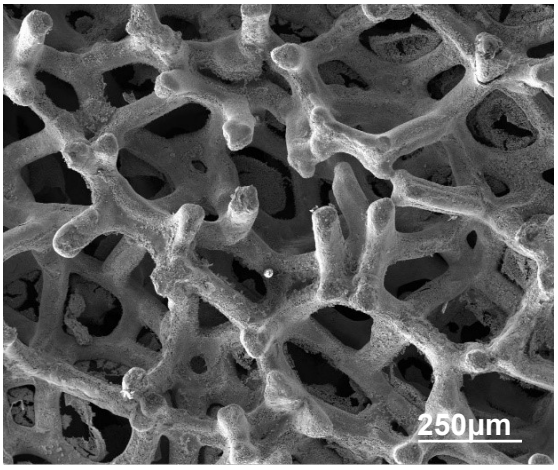

Figure S2. SEM image of Fe foam, showing a porous and interconnected metallic framework.

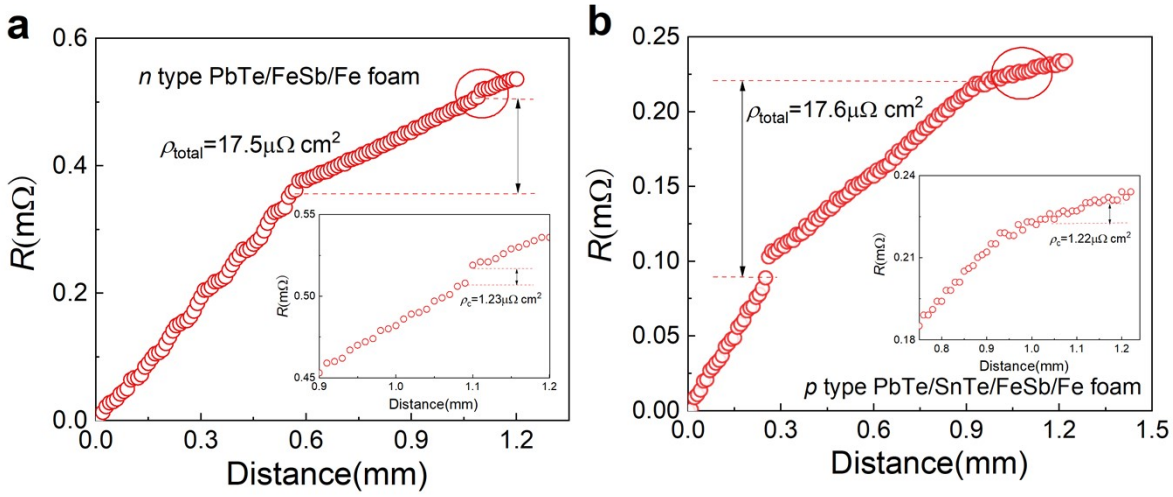

Figure S3. The total interface resistivity (ρ_{total}) at the hot side for the (a) *n*-type and (b) *p*-type thermoelectric legs. The insets show the corresponding interface resistivity for the Fe foam/FeSb joints.

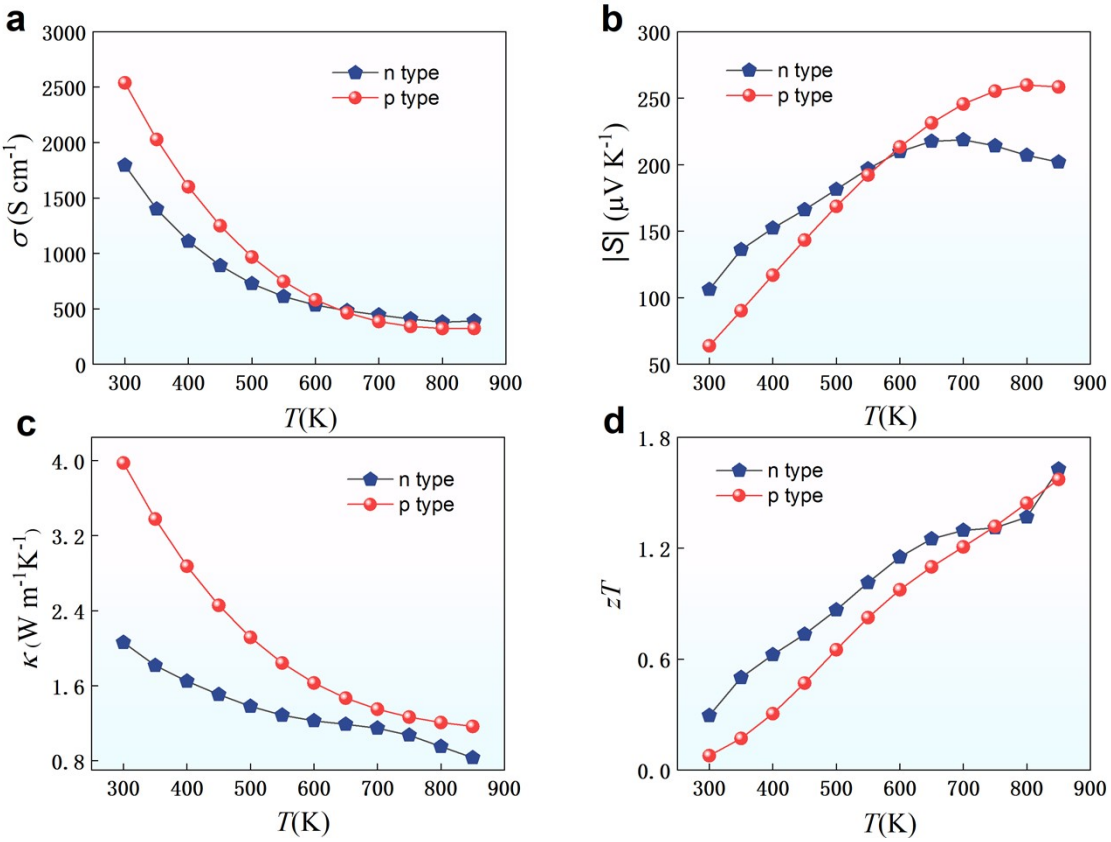

Figure S4. Temperature-dependent thermoelectric properties of *p*-type $Na_{0.02}Pb_{0.98}Te$ and *n*-type $Pb_{0.954}Ge_{0.05}Cu_{0.02}Te_{0.96}Se_{0.04}$. Plotted as a function of temperature are (a) electrical conductivity (σ), (b) the absolute Seebeck coefficient (|S|), (c) thermal conductivity (κ), and (d) the dimensionless figure of merit (*zT*).

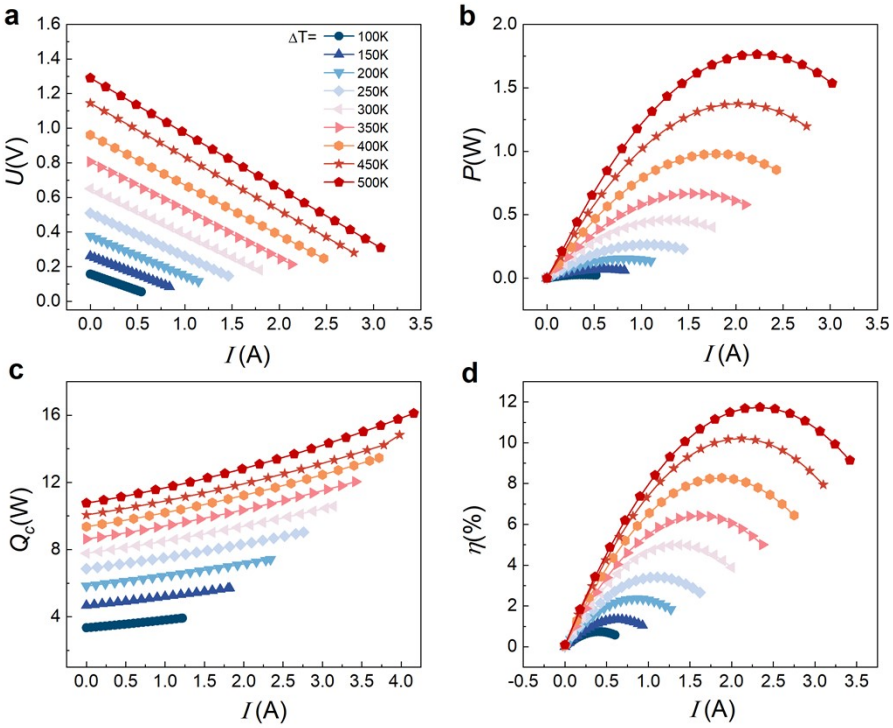

Figure S5. Characterization of the PbTe-based module. Current-dependent (a) output voltage, (b) output power, (c) heat flow out, and (d) efficiency for the module under several temperature differences.

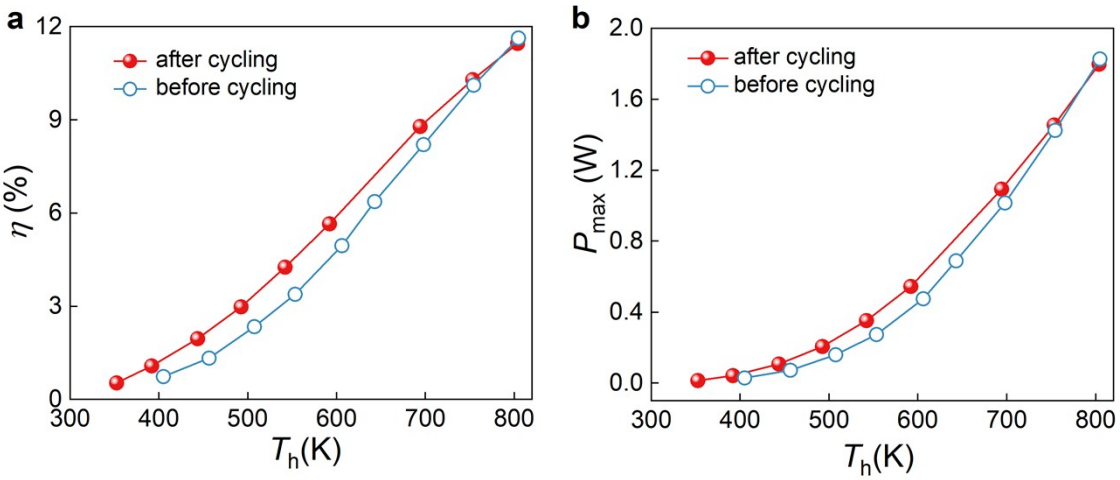

Figure S6. Comparison of (a) conversion efficiency and (b) maximum output power before and after thermal cycling. The results demonstrate that the module performance remains essentially unchanged.

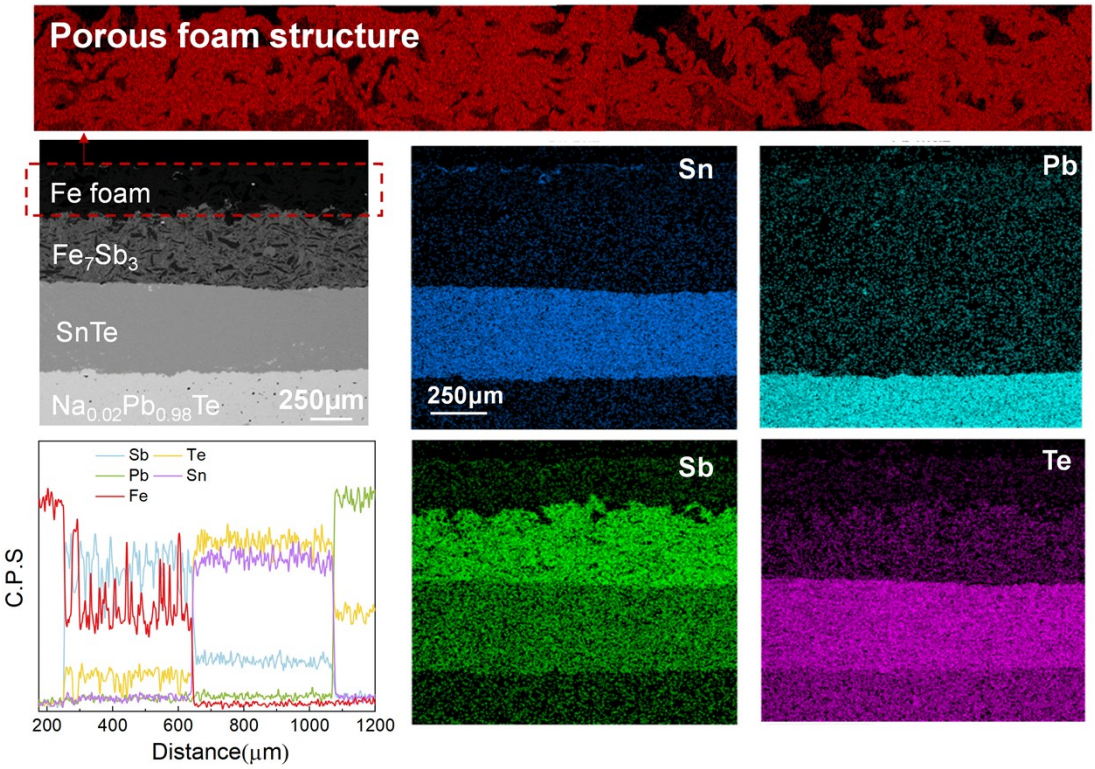

Figure S7. Microstructural and compositional characterization of a hot-side Fe foam/FeSb/SnTe/PbTe junction. The figure presents a scanning electron microscopy image, energy-dispersive X-ray spectroscopy elemental maps, and corresponding EDS line scans.

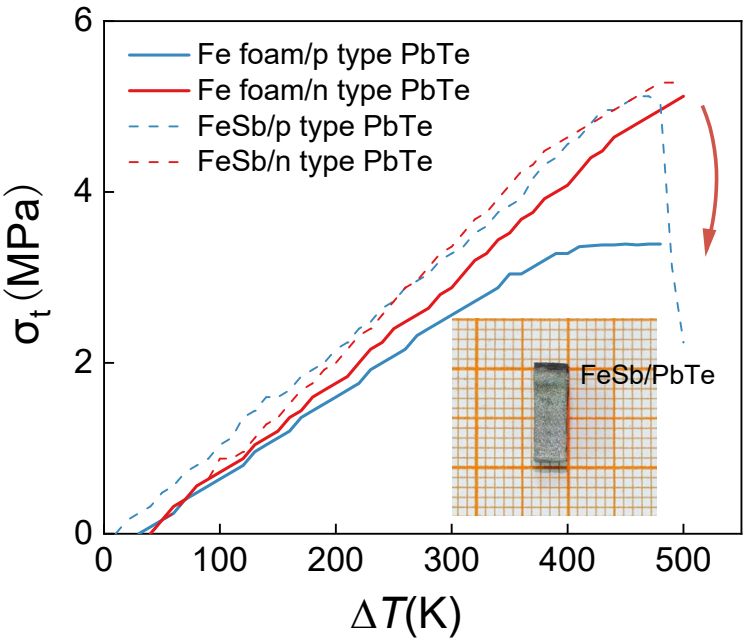

Figure S8. The thermal stress during the heating process of the thermoelectric leg with FeSb/PbTe joint at hot-side and the thermoelectric leg with Fe foam/FeSb joint at hot-side. Inset: A picture of the thermoelectric leg with deformation at hot-side.

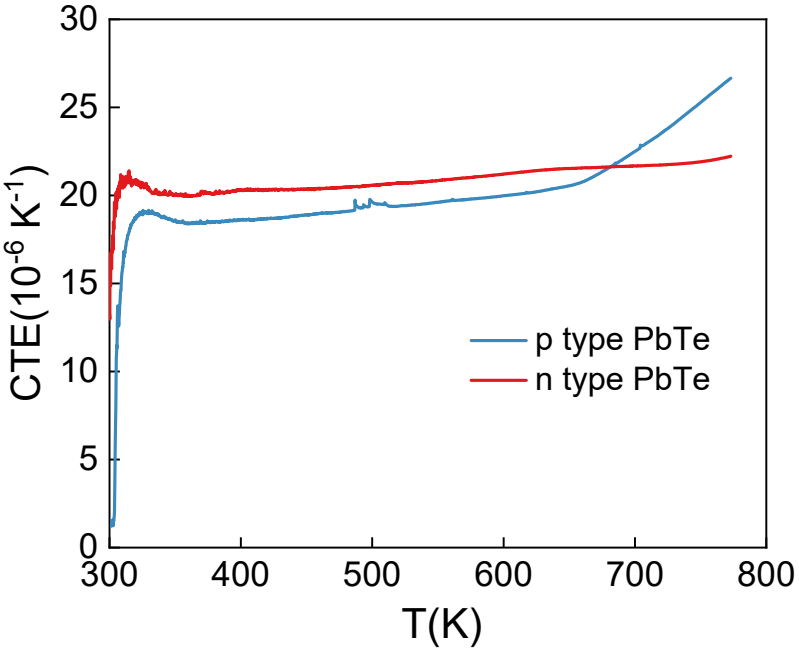

Figure S9. The overall coefficients of thermal expansion for the *p*-type and *n*-type thermoelectric legs. A measurable difference is observed between the two.

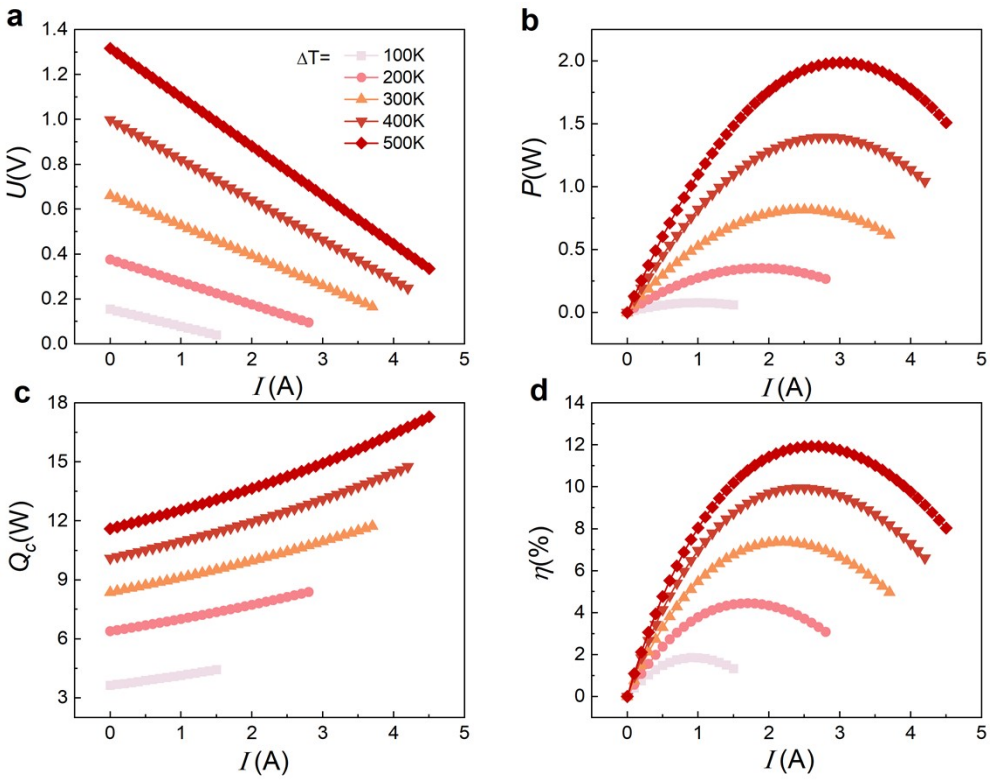

Figure S10. Simulation of the PbTe-based module. Current-dependent (a) output voltage, (b) output power, (c) heat flow out, and (d) efficiency for the module under several temperature differences.

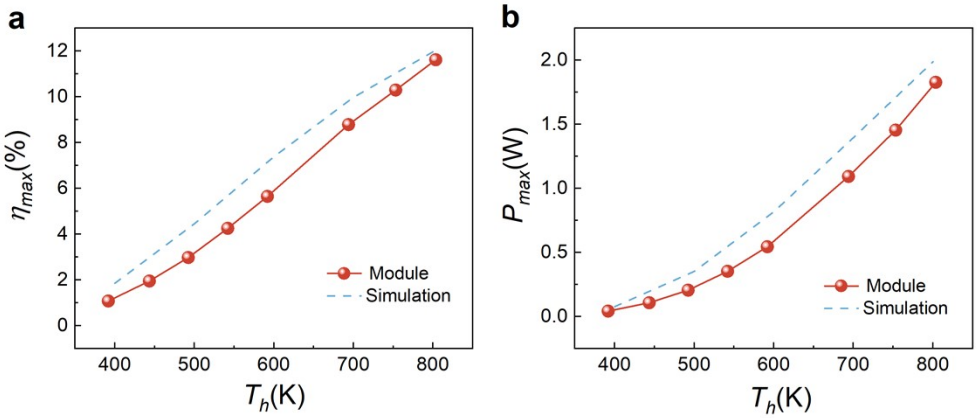

Figure S11. Comparison between measured and simulated properties of the PbTe-based module. (a) maximum efficiency, (b) maximum output power.

Table S1. The relevant material properties used in the simulation of PbTe-based thermoelectric module.

Material	**Cu**	***p*-type PbTe**	***n*-type PbTe**	**FeSb**	**Fe foam**	**SnTe**
σ (S m^{-1})	5.8×10^{7}	323~2538	390~1795	$\sim10^{6}$	$\sim10^{6}$	$\sim10^{5}$
CTE (10^{-6} K^{-1})	17.5~18.5	19.5~21.7	18.5~20.8	12.5~21.3	12~15	19~21.6
C_p (J kg^{-1} K^{-1})	385	190	190	450	450	210
ρ (g cm^{-3})	8.9	7.9	7.8	7.3	4.13	6.4
κ (W m^{-1} K^{-1})	390	1.2~3.9	0.8~2	11~12	11~12	2~3
E (GPa)	110	37~47	33~43	130~150	21~23	40~50
ν	0.35	0.25	0.25	0.27	0.29	0.28